

# Finite-difference full-wave modelling and imaging of different geological structures using staggered-grid approach

Raju Babu Allu<sup>1,2</sup> and Laxmidhar Behera<sup>1,2</sup>

## **ABSTRACT**

Seismic wave propagation through different subsurface geological structures plays a pivotal role for accurate imaging of the target zones of interest. There are several techniques available for numerical simulation of seismic wave propagation through different media. We have used acoustic finitedifference full-wave modelling using staggered-grid approach by employing both free-surface boundary-condition (at top) and perfectly-matched-layer (PML) absorbing-boundarycondition (at other three sides) for the model boundaries. This method is very accurate and computationally efficient for seismic wave propagation and considerably reduces the spurious arrivals mainly occurring due to numerical dispersion, back-scattered noises and multiples. The staggered-grid approach increases spatial resolution and stability of the wavefield simulation, which allow for the efficient propagation of seismic waves in complex subsurface geological structures. We validate the method by running benchmark tests for different models and compared the corresponding results. The results obtained indicate that the method employed is successful in modelling and imaging of flat-horizonal layer and complex geological structures like a gently dipping syncline and anticline model as well as a complex graben model with combination of the above two structures by minimizing the artifacts. We have also reduced the effect of multiple reflections, back-scattered noise, and other spurious arrivals using two-way acoustic wave-equation with free-surface and PML absorbing-boundary-condition constraints, resulting high-quality synthetic seismic data. These synthetic seismic data generated have been further used for efficient imaging by employing the 2-D wave-equation based finite-difference pre-stack depth migration (FDMIG).

## **KEYWORDS**

Finite-difference, full-wave modelling, staggered-grid, absorbing-boundary-conditions, perfectly-matched-layer, wavefield simulation, imaging

## **INTRODUCTION**

Full-wave modelling using acoustic and elastic finitedifference (FD) techniques play pivotal role for subsurface imaging of complex geological structures having steeply dipping target zones, whereas the other generally encounter several different methods problems. The ability to model and accurately simulate seismic wavefield through the complex subsurface geological structures are very important for detecting target zones of interest for hydrocarbon or mineral explorations. Hence, the compute-intensive and robust numerical methods such as acoustic and elastic FD fullwave modelling are very popular now-a-days and increasingly used to address these challenges of imaging complex geological structures amenable for delineating potential zones of hydrocarbon and mineral. The computation generally increases many folds when the subsurface geological structures are heterogeneous and anisotropic in which several numerical phases, backscattered noises and artifacts are generated (Behera and Tsvankin, 2009; Behera, 2022). To handle these issues, suitable perfectly-matched-layer (PML) absorbingboundary-conditions (ABC) and free-surface boundaryconditions are being applied with the staggered-grid FD scheme for both the wavefield simulation and generation of synthetic seismic data. The synthetic seismic data generated using this approach are generally free from surface-waves, multiples and backscattered noises, which are highly dominant in the data when other modelling techniques are used. The main goal of this study is to demonstrate the application of FD method using staggered-grid approach with the help of PML absorbing-boundary-conditions for modelling and simulate the wavefields for a very simple and moderately complex geological models. This will help in the computation of full-wave synthetic seismic data and application of robust and highly compute intensive seismic imaging technique like 2-D wave-equation based finite-difference pre-stack depth migration (FDMIG) for accurate imaging of these geological structures of interest.

<sup>1</sup>CSIR-National Geophysical Research Institute (CSIR-NGRI), Uppal Road, Hyderabad-500007, India

<sup>2</sup>Academy of Scientific and Innovative Research, Uttar Pradesh, Ghaziabad-201002, India

Emails: allu.ngri21j@acsir.res.in; laxmidhar.ngri@csir.res.in

#### **METHODOLOGY**

# Finite-difference modelling

The acoustic finite-difference (FD) method is considered as an efficient approach for wavefield simulation complex through geological structures computation of full-wave synthetic seismic data as compared to other different numerical techniques due to its low computational cost, easy implementation and less computer memory requirements. This method is particularly useful when analytical solutions to wave equations are difficult or impossible to obtain especially in complex models. This technique involves discretizing the continuous partial-differential equations governing the wave propagation through the model grid, where the wavefield values are approximated at discrete points in space and time. For wave propagation through a media, the corresponding wave equation is generally expressed as:

$$\frac{\partial^2 u(x,t)}{\partial t^2} = C^2 \nabla^2 u(x,t) \tag{1}$$

where u(x,t) is the wavefield (such as pressure or displacement), C is the velocity of the waves and  $\nabla^2$  is the Laplacian operator representing the spatial second derivatives. For computational efficiency, the numerical simulations often rely on discretizing the governing equation (Equation 1) using grid systems. These grids can be classified into nonstaggered- and staggered-grid schemes. The main difference between these two approaches relies on how the variables (e.g., velocity and pressure) are positioned on the grids. To understand the finite-difference full-wave modelling procedure and generation of synthetic seismic data, we have presented a flow-chart (Figure 1) to illustrate the different steps involved in modelling having FD kernels along with the shot and time loop for the generation of source wavefield and snapshots of the receiver wavefield followed by storage of the synthetic seismic data. The FD full-wave modelling generally employs two different approaches for wavefield simulation nonstaggered- and staggered-grid for arrangement of the variables (i.e., pressure and velocities) on a numerical mesh. The choice of these two approaches has direct impact on the FD solver for stability, accuracy and ease of implementation.

## Non-staggered-grid approach

A nonstaggered-grid also known as collocated or central-grid (Bartolo et al., 2012) generally stores all the variables in the same grid point. This means that for a 2D problem, the velocity components  $V_x$  and  $V_z$  (for xand z directions) as well as the pressure field P are defined at the same grid point. Hence, the computational grid is easier to set up, since all variables are stored in the same location and direct interpolation of all the variables is possible. Hence, the interpolation of boundary conditions for the source term becomes easier. On the other hand, the disadvantage of nonstaggered-grid scheme is that they suffer from numerical challenges due to the coupling of pressure and velocity fields. Since, the pressure and velocities are estimated at the same grid points, this can lead to problems due to non-physical pressure oscillations causing less numerical stability. Without staggering, the errors in pressure and velocity fields spread very easily, resulting computational instability. For an acoustic medium, the wave equations are generally expressed by the first-order linearized system of Newton's and Hooke's law as (Thorbecke, 2017):

$$\frac{\partial V_x}{\partial t} = -\frac{1}{\rho} \left( \frac{\partial P}{\partial x} \right)$$

$$\frac{\partial V_z}{\partial t} = -\frac{1}{\rho} \left( \frac{\partial P}{\partial z} \right)$$

$$\frac{\partial P}{\partial t} = -\frac{1}{\kappa} \left( \frac{\partial V_x}{\partial x} + \frac{\partial V_z}{\partial z} \right)$$
(2)

where  $V_x$  and  $V_z$  are particle velocity components in x-and z-direction respectively, P is the acoustic pressure,  $\rho$  is the density of the medium and  $\kappa$  is the compressibility.

A basic (nonstaggered) finite-difference grid is used for the acoustic wave equation producing a numerically stable scheme in FD modelling. The nonstaggered-grid scheme takes into account the pressure at discrete locations that are equally spaced in time ( $\Delta t$ ) and spatial direction ( $h=\Delta x=\Delta z$ ). By employing the Taylor-series expansions to obtain the known central-difference operators, each derivative of the wave equation can be roughly calculated. The wave equation for a 2D acoustic media can be expressed as (Bartolo et al., 2012):

$$\frac{\partial^2 P}{\partial t^2} = C^2 \left( \frac{\partial^2 P}{\partial x^2} + \frac{\partial^2 P}{\partial z^2} \right) + F(x, z, t) \tag{3}$$

The corresponding second-order approximations of the above wave equation (Equation 3) can be expressed as:

$$\frac{\partial^{2} P}{\partial t^{2}} = \frac{P_{i,j}^{n-1} - 2P_{i,j}^{n} + P_{i,j}^{n+1}}{\Delta t^{2}}, 
\frac{\partial^{2} P}{\partial x^{2}} = \frac{P_{i-1,j}^{n} - 2P_{i,j}^{n} + P_{i+1,j}^{n}}{\Delta x^{2}}, 
\frac{\partial^{2} P}{\partial z^{2}} = \frac{P_{i,j-1}^{n} - 2P_{i,j}^{n} + P_{i,j+1}^{n}}{\Delta z^{2}}$$
(4)

where P is the wave propagation in the x, z, t and F(x,z,t) is the corresponding source wavefield. The grid spacing in x and z direction is represented as  $\Delta x$  and  $\Delta z$  having traveltime interval of  $\Delta t$  with n as the number of discrete time steps (i.e.,  $t=n\Delta t$ ) and C as the velocity of the waves through the media. The source time function used is the Ricker wavelet. After simplification of equation (4), the final nonstaggered-grid pressure wavefield for the acoustic media can be expressed as:

$$P_{i,j}^{n+1} = \frac{\Delta t^2}{\Delta x^2} * C^2(i,j) * \left[ P_{i-1,j}^n - 2P_{i,j}^n + P_{i+1,j}^n \right] + \frac{\Delta t^2}{\Delta z^2} * C^2(i,j) * \left[ P_{i,j-1}^n - 2P_{i,j}^n + P_{i,j+1}^n \right] + F(x,z,t) * \Delta t^2 + 2P_{i,j}^n - P_{i,j}^{n-1}$$
 (5)

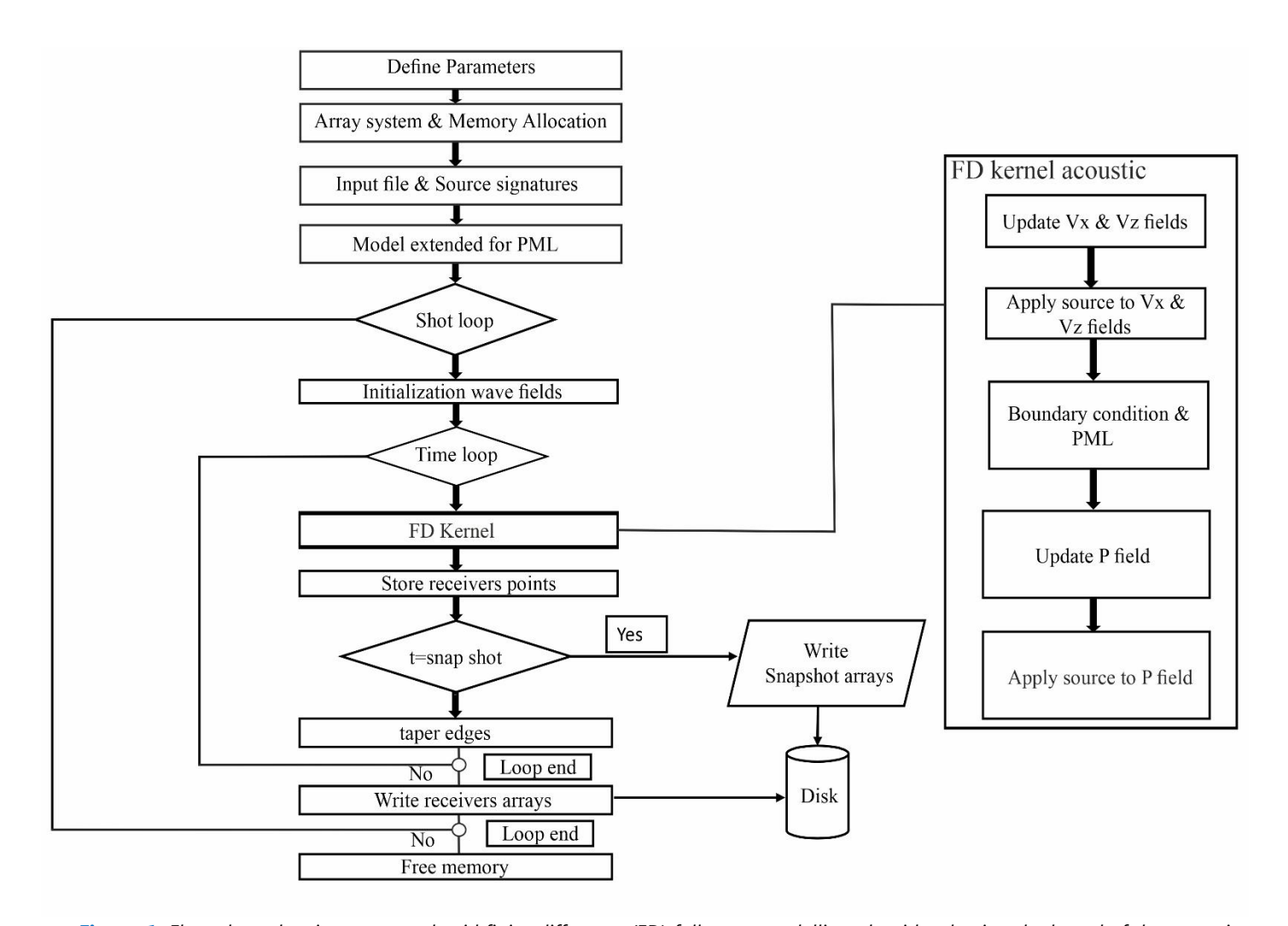


**Figure 1:** Flow-chart showing staggered-grid finite-difference (FD) full-wave modelling algorithm having the kernel of the acoustic scheme used for wavefield simulation and generation of synthetic seismic data. The two decision loops are for the number of shot positions and the number of time-steps to be modelled. In the flow-chart, the time is represented by t, horizontal and vertical particle velocity by  $V_x$  and  $V_z$ , respectively, and P is the acoustic pressure.

## Staggered-grid approach

In staggered-grid approach, the variables such as velocity and pressure are defined not only at grid points, but also at half-grid points (Virieux, 1984, 1986; Graves, 1996, Behera, 2022). Hence, the velocity and pressure components are set to different spatial positions as shown in Figure 2. For example, the grids of velocity components  $V_x$  and  $V_z$  wavefields are positioned in between the P grid. This method has advantages of improved accuracy and stability in seismic wave simulations. Staggering the velocity and pressure fields eliminate the pressure oscillations as compared to

nonstaggered-grid approach, resulting in greater stability and computational efficiency of wave field simulations. Staggered-grids have low numerical dispersion of waves as compared to nonstaggered-grids. However, the staggered-grids demand more complex interpolation and boundary-conditions. It can be more difficult to build a staggered-grid than a nonstaggered one, especially in irregular domains. We have shown how the FD kernels are used to compute update for  $V_x$  and  $V_z$  along with the kernel to compute update of P using staggered-grid implementation scheme (Figure 2).

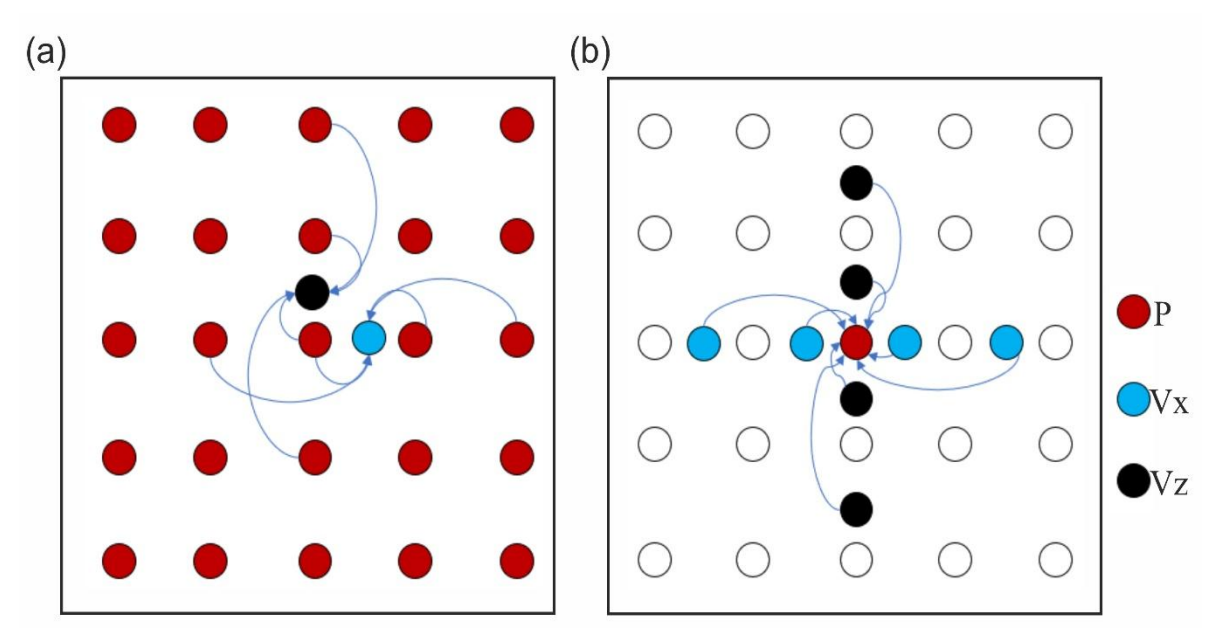


**Figure 2:** The staggered-grid representation of the compute kernels showing grid-points (open and filled circles) needed to update the (a)  $V_x$  and  $V_z$ , and (b) pressure (P) wavefields. The wavefields all have unique grid position. This indicates that the grids of  $V_x$  and  $V_z$  wavefields are located in between the P grid.

The corresponding first-order derivatives in the spatial coordinates (lateral position x and depth position z) of equation (2) are approximated by the centralized fourth-order Crank-Nicolson approximation as (Thorbecke, 2017):

$$\frac{\partial P}{\partial x} \approx \frac{-P\left(\left(i+\frac{3}{2}\right)\Delta x\right) + 27P\left(\left(i+\frac{1}{2}\right)\Delta x\right) - 27P\left(\left(i-\frac{1}{2}\right)\Delta x\right) + P\left(\left(i-\frac{3}{2}\right)\Delta x\right)}{24\Delta x} \tag{6}$$

$$\frac{\partial P}{\partial z} \approx \frac{-P\left(\left(k + \frac{3}{2}\right)\Delta z\right) + 27P\left(\left(k + \frac{1}{2}\right)\Delta z\right) - 27P\left(\left(k - \frac{1}{2}\right)\Delta z\right) + P\left(\left(k - \frac{3}{2}\right)\Delta z\right)}{24\Delta z}$$
(7)

The first-order derivative in time is approximated by a second-order scheme as:

$$\frac{\partial P}{\partial t} \approx \frac{-P\left(\left(i + \frac{1}{2}\right)\Delta t\right) - P\left(\left(i - \frac{1}{2}\right)\Delta t\right)}{\Delta t} \tag{8}$$

These approximations can be derived from linear combination of different Taylor-series expansions (Fornberg, 1988). These above equations are being implemented in the finite-difference code using a staggered-grid scheme, which follow the grid layout as described by Virieux (1986). The implementation of equation (2) is also called a stencil, since it forms a pattern of four grid point needed to compute the partial-derivative at one grid point (Figure 2b). To

compute the spatial derivative on all grid points, the stencil is shifted through the grid (Figure 2a).

The model parameters used in the finite-difference program are

$$(\lambda + 2\mu) = V_p^2 \rho = \frac{1}{\kappa} \tag{9}$$

where  $\rho$  is the density of the medium,  $V_p$  is the P-wave (compressional) velocity,  $\lambda$  and  $\mu$  are the Lame parameters and  $\kappa$  is the compressibility. The program reads the P-wave velocity and density of the medium as gridded input model files. From these files, the program computes the Lame parameters used in the first-order equations (Equation 1) to compute the wavefield at next time-steps (Thorbecke, 2017).

$$V_{x_{i+\frac{1}{2}k}}^{n+\frac{1}{2}} = V_{x_{i+\frac{1}{2}k}}^{n-\frac{1}{2}} - b_{i+\frac{1}{2}k} \left(\frac{\Delta t}{h}\right) \left(P_{i+1,k}^{n} - P_{i,k}^{n}\right)$$
(11)

$$V_{z_{i,k+\frac{1}{2}}}^{n+\frac{1}{2}} = V_{z_{i,k+\frac{1}{2}}}^{n-\frac{1}{2}} - b_{i,k+\frac{1}{2}} \left(\frac{\Delta t}{h}\right) \left(P_{i,k+1}^n - P_{i,k}^n\right) \tag{12}$$

$$P_{i,k}^{n+1} = P_{i,k}^{n} - \kappa_{i,k} \left( \frac{\Delta t}{h} \right) \left\{ \left( V_{x_{i+\frac{1}{2},k}}^{n+\frac{1}{2}} - V_{x_{i-\frac{1}{2},k}}^{n+\frac{1}{2}} \right) + \left( V_{z_{i,k+\frac{1}{2}}}^{n+\frac{1}{2}} - V_{z_{i,k-\frac{1}{2}}}^{n+\frac{1}{2}} \right) \right\} + F(x,z,t)$$

$$(13)$$

where  $V_x$  and  $V_z$  are the particle velocities in each direction (x and z) and b is the buoyancy (inverse of density  $1/\rho$ ) at the staggered-grid positions,  $\Delta t$  is the traveltime interval and h (i.e.,  $\Delta x = \Delta z$ ) is the grid spacing in both x and z directions, n is the integer indices of the number of time-steps and F(x,z,t) is the source wavefield.

# Stability conditions

The equations (6) to (8) use finite-difference operators to approximate the first-order differential equations. When explicit time-marching strategies are utilized in numerical solutions, the Courant (Courant et al., 1967) number provides a convergence criterion. The Courant number is a dimensionless quantity used in FD modelling to ensure the stability and accuracy of the solution. It represents the ratio of the time-step size to the spatial grid spacing relative to the wave speed within the system. The Courant number limits the time-step in explicit time-marching computer simulations. To simulate a wave spanning a discrete grid distance ( $\Delta x$  or  $\Delta z$ ), the time-step must be smaller than the time it takes to reach an adjacent grid point. Otherwise, the

To obtain the second-order partial-derivatives in space and time, the central-difference operator of the form (Bartolo et al., 2012)

$$\frac{dg_{i,k}^n}{dx} = \frac{g_{i+\frac{1}{2},k}^n - g_{i-\frac{1}{2},k}^n}{h} \tag{10}$$

is applied to approximate the derivatives in equations (1) and (2) at the correct positions shown in Figure 2, where g is the field of propagation (or its components) in the medium  $(P, V_x \text{ or } V_z)$  along x and z directions. The second-order standard staggered-grid acoustic wavefields of the medium can be expressed as (Bartolo et al., 2012):

simulation will yield inaccurate results. As grid point separation reduces, the upper time-step limit of the wavefield simulation also diminished. For the fourth-order spatial derivatives, the Courant number is 0.606 (Sei, 1995) so that the discretization becomes stable. The stability criteria of the fourth-order approximation proposed by Levander (1988) can be expressed as:

$$\Delta t < 0.606 \left( \frac{\Delta x (=\Delta z)}{V_{p,max}} \right) \tag{14}$$

Equation (14) is obtained from the general stability criteria for a 2D regular staggered-grid ( $\Delta x = \Delta z$ ) explicit finite-difference scheme of Behera (2022) as:

$$\Delta t < \frac{1}{\sqrt{2}} \left( \frac{\Delta x (= \Delta z)}{V_{n,max}} \right) \frac{1}{\sum_{m=1}^{M} |a_m|}$$
 (15)

where M is the half of the differential operator length and  $a_m$  is the finite-difference coefficients of 9/8 and 1/24, respectively (Levander, 1988). To attenuate the energy generated due to artificial reflections from the side and bottom of the model, a suitable perfectly-matched-layer (PML) absorbing-boundary-conditions need to be imposed in the modelling algorithm. The schematic sketch (Figure 3) show how the damping

parameters (D) are set within the model grids for successful implementation of the PML absorbing-boundary-condition (Collino and Tsogka, 2001). Also, free-surface boundary-condition for the top and PML absorbing-boundary-condition for the other three sides of the model are necessary for efficient wave propagation and generation of full-wave synthetic seismic data (Behera, 2022). We have demonstrated the application of different types of boundary-conditions for the selected models in this study for wavefield simulation and corresponding effect on FD modelling and synthetic seismic data generation.

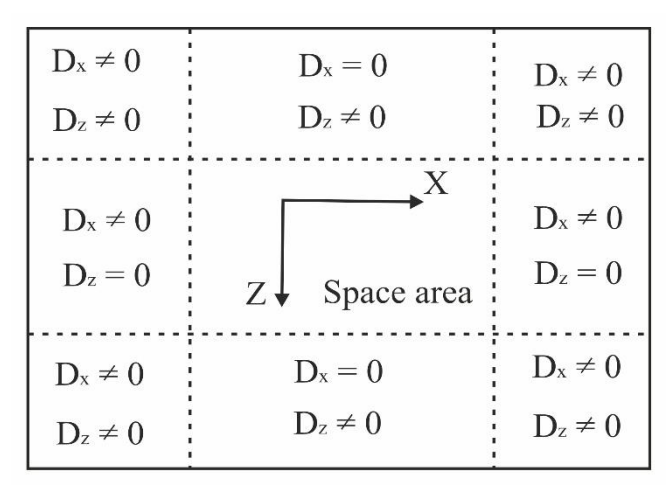


**Figure 3:** The damping functions (D) in four-sides and four corners of PML.  $D_x$  has non-zero values at the left and right absorbing layers while  $D_z$  has non-zero values at the top and bottom absorbing layers. The non-zero value increases with the increase of distance from the inner boundaries of the absorbing layers, which are indicated by the dashed lines.

## **FULL-WAVE SYNTHETIC SEISMIC DATA**

We have employed the acoustic finite-difference modelling using staggered-grid approach for wavefield simulation and generation of full-wave synthetic seismic data for (a) a very simple flat-horizontal two-layer model, (b) a moderately complex geological model consisting a series of alternate synclines and anticlines called syncline and anticline model, and (c) a complex geological model with combination of the above two features along with a graben and flat-horizontal layer below them called a complex graben model. The acoustic full-wave synthetic seismic data generated for these three models are used for seismic imaging in this study.

## (a) Flat-horizontal model

The simplest model used for implementation of the acoustic FD modelling using the staggered-grid scheme with application of different boundary-conditions is the flat-horizontal two-layer model (Figure 4). The model is considered as homogeneous and isotropic having single interface at 1.0 km depth (Figure 4). All the model parameters used for wavefield simulation and computation of full-wave synthetic seismic data are presented in Table-1.

## Wavefield simulation

For the acoustic wave propagation and computation of full-wave synthetic seismic data through the isotropic media using staggered-grid FD modelling scheme (Figure 3), it is very important to understand the nature of wave propagation by wavefield simulation at different time-steps without application any boundary-condition and application of different boundary-conditions like free-surface boundary-condition, free-surface with absorbing-boundary-condition and free-surface with PML absorbing-boundary-condition for the flat-horizontal model (Figure 5). We have presented the wavefield simulation for the shot location at 2 km of the flat-horizontal model (Figure 4).

At the time-step of 0.5 s, the corresponding snapshots of the wave propagation show very simple without any distortion of the wavefield through the model using no boundary-condition (Figure 5a), free-surface boundarycondition (Figure 5b), free-surface with absorbingboundary-condition (Figure 5c) and free-surface with PML absorbing-boundary-condition (Figure Similarly, at increasing time-steps of 1.0 s, the corresponding snapshots of wave propagation show the nature of wavefield using the above-mentioned boundary-conditions (Figure 5e-h) in which the freesurface with PML absorbing-boundary-condition snapshot (Figure 5h) minimizes all the spurious arrivals, back-scattered noises, multiples and distortion of waves as compared to the snapshots of wave propagation using other three boundary-conditions (Figure 5e-g). At increasing time steps of 1.5 s, we can observe that there is more complexity of wavefield leading to spurious arrivals present in the snapshots of wave propagation with no boundary-condition (Figure 5i), free-surface boundary condition (Figure 5j), free-surface with absor-

**Table-1**: Acoustic finite-difference full-wave modelling parameters

Model parameters	Flat-horizontal layer model	Syncline and anticline model	Complex graben model
Dimension ( $x$ and $z$ )	$4 \text{ km} \times 2 \text{ km}$	$4 \text{ km} \times 2 \text{ km}$	$3 \text{ km} \times 1.5 \text{ km}$
Number of samples in $x$ and $z$ ( $nx$ and $nz$ )	400 × 200	400 × 200	600 × 300
Grid spacing in $x$ and $z$ ( $dx$ and $dz$ )	10 m × 10 m	10 m × 10 m	5 m × 5 m
Frequency of source wavelet (Ricker) in Hz	20	20	20
Sampling interval $dt$ (ms)	2	2	4
Record length (s)	2	2	1.5
Number of time samples (ns)	1000	1000	375
Velocity $V_P$ (m/s)	2000, 4000	2000, 4000	1500, 2500, 3500, 2000, 5500
Density $\rho$ (g/cm <sup>3</sup> )	2.2	2.2	1.4, 2.2, 2.4, 2.1, 2.8
Shot interval (m)	100	100	50
Receiver interval (m)	20	20	20
Total number of shots	31	31	47
Number of receivers per shot	201	201	151
First shot location (m)	500	500	500
Last shot location (m)	3500	3500	2800



**Figure 4:** Isotropic flat-horizontal two-layer model having a single reflecting interface used for acoustic FD modelling and simulation using staggered-grid scheme (Figure 1) for computation of full-wave synthetic seismic data and imaging. The velocity of the two layers are 2000 m/s and 4000 m/s with constant density of 2.2 g/cm³ having maximum depth of the model is 2 km and maximum horizontal distance of the model is 4 km. The velocity variation of the model is shown in color scale.

bing-boundary-condition (Figure 5k) as compared to free-surface with PML absorbing-boundary-condition (Figure 5I). The snapshot having free-surface with PML absorbing-boundary-condition has clear down-going waves, reflected waves with very good absorption of all the spurious arrivals or noises and other numerical waves generated during FD modelling (Figure 51). Similarly, at the final time-step of 2.0 s, the corresponding snapshot of the wave propagation should be free from any arrivals, and the wavefield should be distortionless. However, we could see some numerical phases and distortion of the wavefield in the snapshots with no boundary-condition (Figure 5m), free-surface boundary-condition (Figure 5n), freesurface with absorbing-boundary-condition (Figure 50) as compared to free-surface with PML absorbingboundary-condition (Figure 5p) for the propagation through the media. Hence, we can observe that, there is no leakage of waves as well as complete absorption of unwanted arrivals and numerical phases generated due to FD modelling using the staggeredgrid scheme in case of free-surface with PML absorbing-boundary-condition snapshots (Figure 5d, h, l, p) of wavefield simulation through the very simple flathorizontal layer model (Figure 4).

The full-wave synthetic seismic data generated after complete wavefield simulation using no boundarycondition, free-surface boundary-condition, surface with absorbing-boundary-condition and freesurface with PML absorbing-boundary-condition are shown in Figure 6. We can observe the presence of different arrivals for a simple two-layer model having a single reflector at 1.0 km depth (Figure 4) for the example shot location at 2.0 km distance for which the wavefield simulation has been presented (Figure 5). The synthetic seismic data obtained without application of any boundary-condition for the simple flat-horizontal model having one reflecting interface (Figure 4) show various arrivals like back-scattered noises, multiples, and other spurious waves superimposed on the data having direct arrivals and reflection phase (Figure 6a).

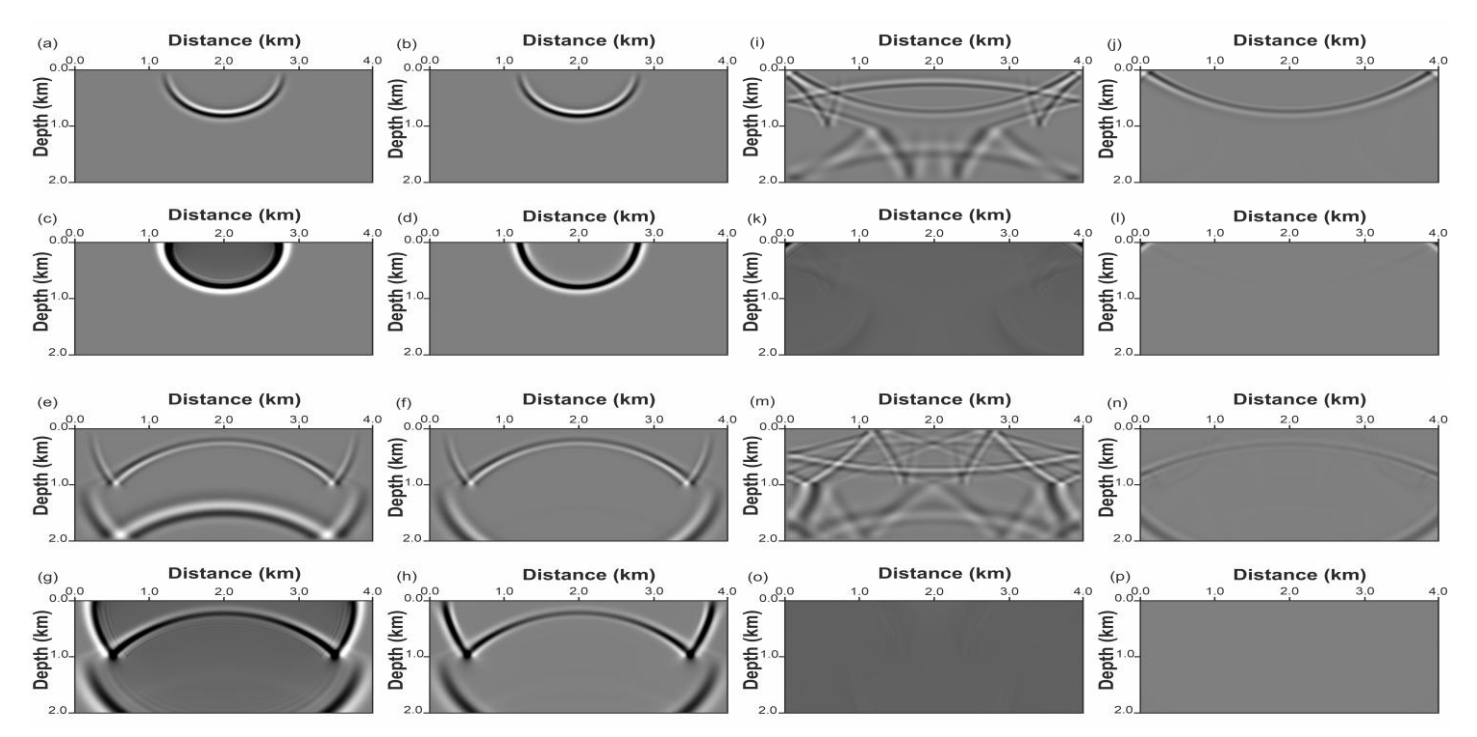


**Figure 5:** The snapshots of the wavefield simulation presented for the flat-horizontal model (Figure 4) at different time-steps by employing (a) no boundary-condition, (b) free-surface boundary-condition, (c) free-surface with absorbing-boundary-condition, (d) free-surface with perfectly-matched-layer (PML) absorbing-boundary-condition for the wave propagation at 0.5 s through the model. Similarly, the corresponding wave propagations at 1.0 s with the above-mentioned boundary conditions are shown in panels (e) to (h), at 1.5 s in panels (i) to (l), at 2.0 s in panels (m) to (p), respectively for the flat-horizontal two-layer media.

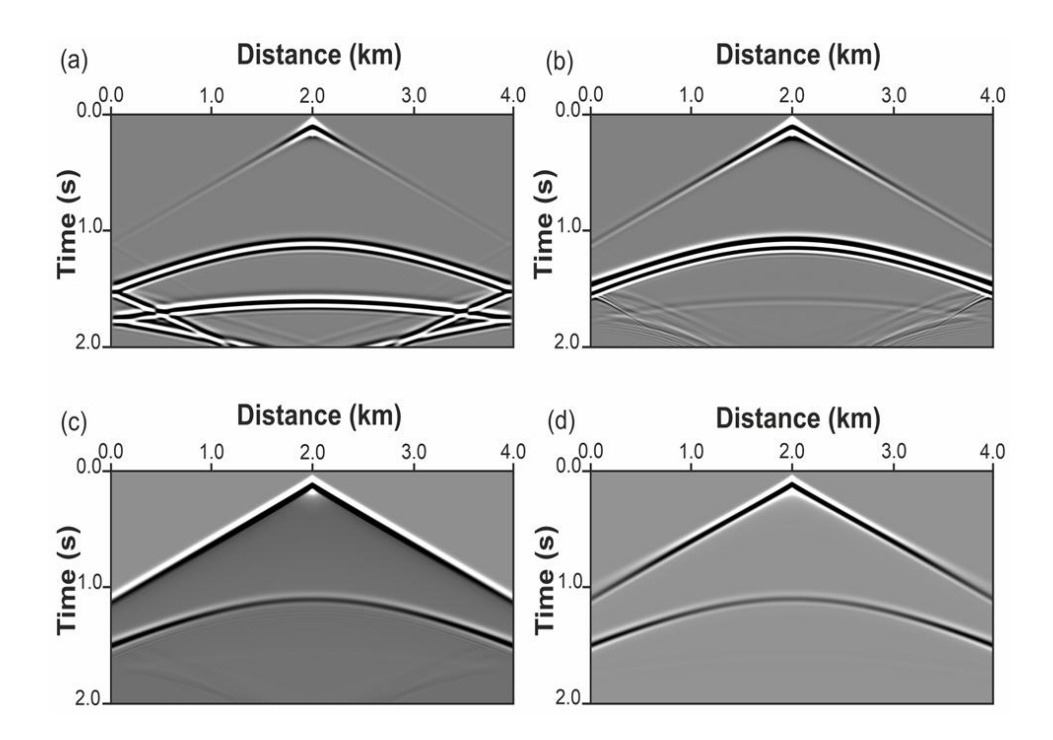


**Figure 6:** The acoustic full-wave synthetic seismic data computed at 2.0 km of the flat-horizontal model (Figure 4) using the staggered-grid FD modelling scheme by employing (a) no boundary-condition, (b) free-surface boundary-condition, (c) free-surface with absorbing-boundary-condition, and (d) free-surface with PML absorbing-boundary-condition, respectively to show the data quality and presence of different arrivals for this very simple model having single reflecting interface.

However, the effect of these spurious arrivals and noises present in the data diminishes with application of freesurface boundary-condition (Figure 6b), free-surface with absorbing-boundary-condition (Figure 6c) and free-surface with PML absorbing-boundary-condition (Figure 6d). The data quality is very good without any spurious arrivals or noises in case of free-surface with PML absorbing-boundary-conditions applied to the FD modelling (Figure 6d). This indicates that the application of acoustic FD full-wave modelling using staggered-grid scheme by employing free-surface with PML absorbingboundary-condition can generate full-wave synthetic seismic data free from unwanted arrivals or noises (Figure 6d), which generally obscure the data by using other boundary-conditions (Figure 6a-c). Hence, this is a direct test of the efficacy of this method for a simple benchmark flat-horizontal model having single reflecting interface (Figure 4).

## (b) Syncline and anticline model

The application of staggered-grid FD full-wave modelling by employing different boundary-conditions

has been tested for a more complex and geologically plausible syncline and anticline model (Figure 7), which is considered as one of the favourable target zones for hydrocarbon exploration. The model is considered as homogeneous and isotropic having single interface as alternate syncline and anticline starting at 1.0 km depth (Figure 7). The detail model parameters of the syncline and anticline model used for acoustic FD modelling are presented in Table-1.

## Wavefield simulation

The corresponding wavefield simulation through the alternate syncline and anticline model (Figure 7) by employing the acoustic staggered-grid FD modelling is shown in Figure 8. The wavefield simulation at the same shot location of 2.0 km distance for this alternate syncline and anticline model (Figure 8) is presented. At the time-step of 0.5 s, the corresponding snapshots of the wave propagation through the model show very simple semi-circular wave-front without any distortions using no boundary-condition (Figure 8a), free-surface boundary-condition (Figure 8b), free-surface with absorbing-boundary-condition (Figure 8c) and free-

surface with PML absorbing-boundary-condition (Figure 8d) because the wave propagation is acoustic and

confined within the first-layer, which is isotropic and homogeneous.

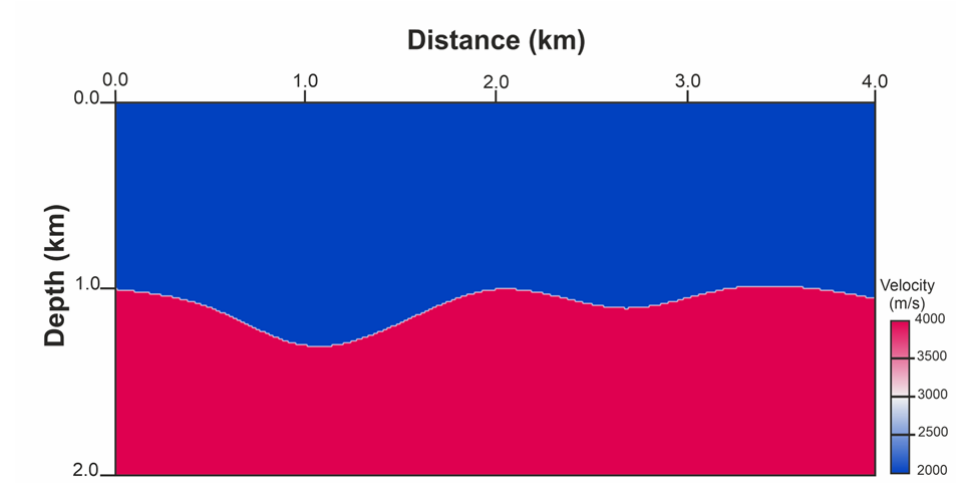


**Figure 7:** The isotropic syncline and anticline model having a single reflecting interface used for computation of full-wave synthetic seismic data and imaging using the same FD modelling scheme (Figure 1). The velocity of the two layers are 2000 m/s and 4000 m/s with constant density of 2.2 g/cm<sup>3</sup> having maximum depth of the model is 2 km and maximum horizontal distance of the model is 4 km. The velocity variation of the model is shown in color scale.

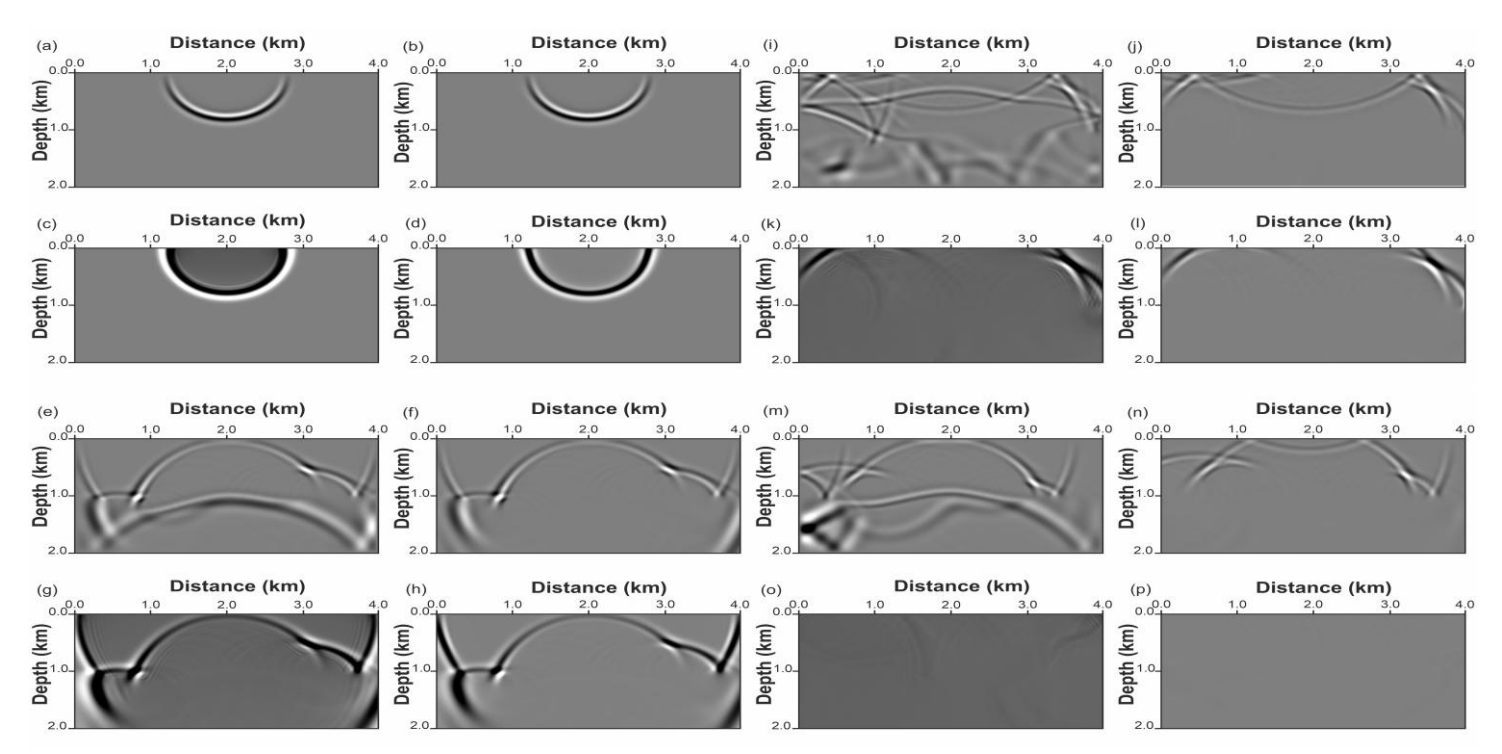


**Figure 8:** The corresponding snapshots are shown for the syncline and anticline model (Figure 7) at different time-steps of the wavefield simulation by employing the same (a) no boundary-condition, (b) free-surface boundary-condition, (c) free-surface with absorbing-boundary-condition, and (d) free-surface with perfectly-matched-layer (PML) absorbing-boundary-condition for the wave propagation at 0.5 s through the model. Similarly, the snapshots of the wave propagations at 1.0 s with the above-mentioned boundary-conditions are shown in panels (e) to (h), at 1.5 s in panels (i) to (l), at 2.0 s in panels (m) to (p), respectively for this two-layer model.

However, at time-step of 1.0 s, the corresponding snapshots of wave propagation show very complex nature of wavefield overlapped with different type of noises and spurious arrivals, which are superimposed on the reflections from the interface of the syncline and anticline model (Figure 7) with application of all the above-mentioned boundary-conditions (Figure 8e-h). It is clearly observed that, the snapshot of the wavefield using free-surface with PML absorbing-boundarycondition (Figure 8h) minimizes all the spurious arrivals, back-scattered noises, multiples and other distortions of waves as compared to the corresponding snapshots of wave propagation using other three boundaryconditions (Figure 8e-g). At increasing time steps of 1.5 s, we can see that there is more complexity of wavefield leading to spurious arrivals present in the snapshots of wave propagation having application of no boundarycondition (Figure 8i), free-surface boundary-condition (Figure 8j), free-surface with absorbing-boundarycondition (Figure 8k) as compared to free-surface with PML absorbing-boundary-condition (Figure 8I). The wavefield snapshot generated at 1.5 s show very clear down-going waves and reflected waves with complete

absorption of unwanted waves or noises using freesurface with PML absorbing-boundary-condition (Figure 8l) for the acoustic staggered-grid FD modelling. Similarly, at the final time-step of 2.0 s, the corresponding snapshot of the wave propagation should be free from any arrivals, which should be blank similar to the flat-horizontal model. However, we could see some numerical phases and distortion of the wavefield in the snapshots with application of no boundary-condition (Figure 8m), free-surface boundary condition (Figure 8n), free-surface with absorbingboundary-condition (Figure 8o) as compared to freesurface with PML absorbing-boundary-condition (Figure 8p) for the wave propagation through the media. This clearly demonstrates that in spite of increasing complexity of the model, there is no leakage of waves as well as complete absorption of unwanted arrivals and numerical phases generated due to FD modelling using the staggered-grid scheme in the case of free-surface with PML absorbing-boundary-condition (Figure 8d, h, I, p) snapshots of the wave propagation through the complex syncline and anticline model.

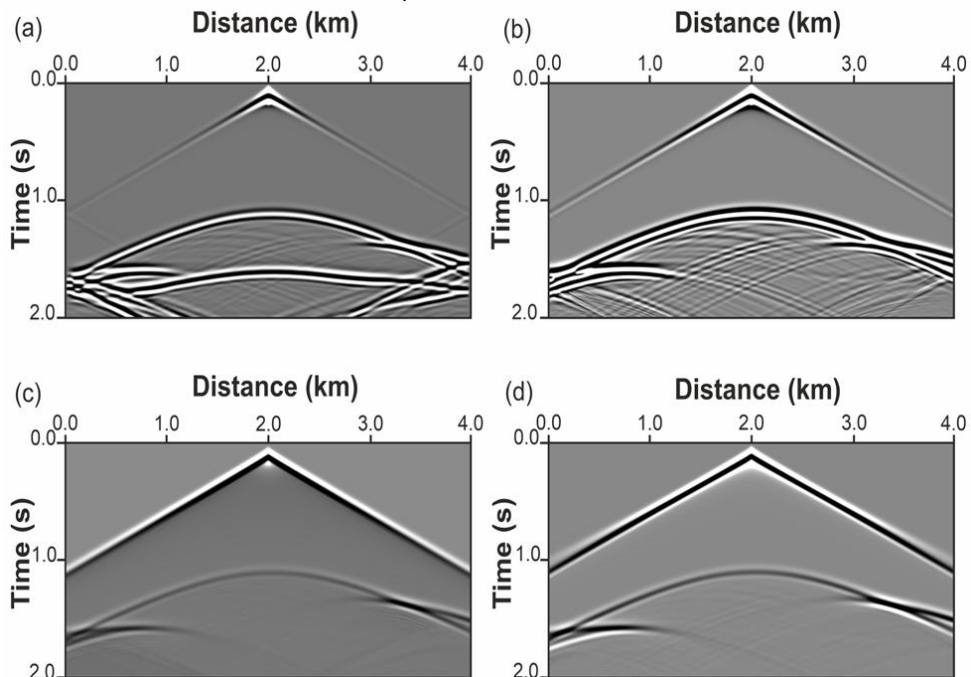
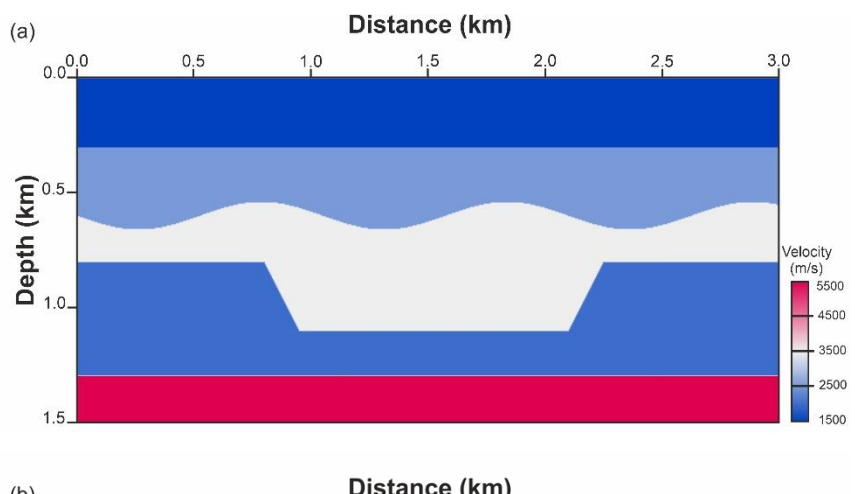


Figure 9: The acoustic full-wave synthetic seismic data computed for the shot at 2.0 km of the syncline and anticline model (Figure 7) using the staggered-grid FD modelling scheme (Figure 1) by employing (a) no boundary-condition, (b) free-surface boundary-condition, (c) free-surface with absorbing-boundary-condition, and (d) free-surface with PML absorbing-boundary-condition, respectively. The synthetic seismic data show nature of different arrivals for the simple syncline and anticline model having single reflecting interface.

The full-wave synthetic seismic data generated after complete wavefield simulation at the same shot location of 2.0 km using no boundary-condition, free-surface boundary-condition, free-surface with absorbingboundary-condition and free-surface with PML absorbing-boundary-condition are shown in Figures 9a to d). We can observe the presence of different arrivals in the synthetic seismic data obtained for the complex two-layer syncline and anticline model having a single reflector starts at 1.0 km depth (Figure 7). The synthetic seismic data obtained without application of any boundary-condition for this model having one reflecting interface (Figure 7) show various arrivals like backscattered noises, multiples, and other numerical phases along with the direct arrivals and reflection phase (Figure 9a).

However, the effect of these spurious arrivals, multiples and noises present in the data diminishes with

application of free-surface boundary-condition (Figure 9b), free-surface with absorbing-boundary-condition (Figure 9c) and free-surface with PML absorbingboundary-condition (Figure 9d). The quality of synthetic seismic data generated by employing free-surface with PML absorbing-boundary-condition (Figure 9d) is considered as the best representing the data corresponding to the true nature of syncline and anticline model without any unwanted spurious arrivals or noises as compared to other three data sets (Figure 9a-c). Hence, the acoustic FD full-wave modelling using staggered-grid scheme and employing the free-surface with PML absorbing-boundary-condition can generate good quality full-wave synthetic seismic data (Figure 9d) required for seismic imaging as compared to the data obtained with application of other boundary-conditions (Figure 9a-c).



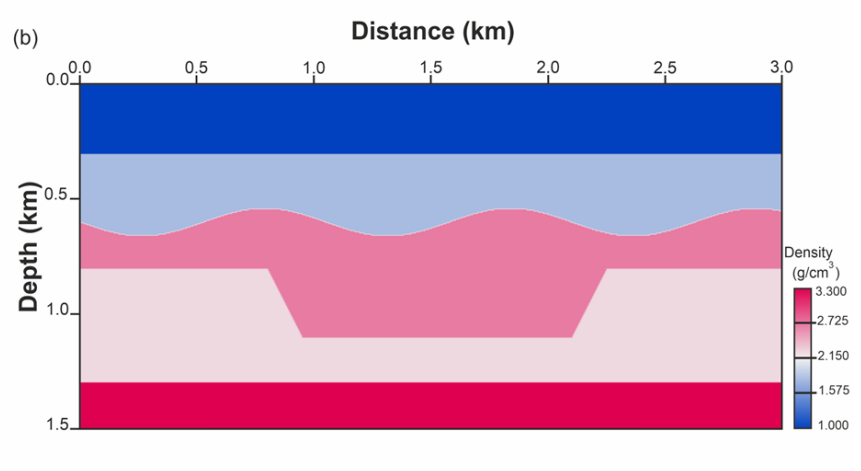


Figure 10: (a) A five-layer acoustic, isotropic and laterally-homogeneous complex graben model having four different reflecting interfaces is used for computation of full-wave synthetic seismic data and imaging with the help of same FD modelling scheme (Figure 1). The corresponding velocities of the five-layers are 1500 m/s, 2500 m/s, 3500 m/s, 2000 m/s, and 5500 m/s with (b) variable densities of 1.4 g/cm³, 2.2 g/cm³, 2.4 g/cm³, 2.1 g/cm³, and 2.8 g/cm³, respectively for the five-layers from top to bottom having maximum depth of the model is 1.5 km and maximum horizontal distance of the model is 3 km. The velocity variation of the model is shown in color scale.

# (c) Complex graben model

To show the efficacy of the staggered-grid FD full-wave modelling by using different boundary-conditions, we have also employed this method for a complex graben model (Figure 10) with corresponding model parameters defined in Table-1. We have simulated the model with 5 m grid-size for both x- and z-directions having receiver interval of 20 m and source interval of 50 m for the wave propagation through the model using the 20 Hz Ricker wavelet for the source. The full-wave synthetic seismic data is generated for the complex graben model by employing acoustic staggered-grid FD wavefield simulation with SI of 4 ms and corresponding record length of 1.5 s. The detail model parameters are presented in Table-1 used for acoustic FD modelling and computation of full-wave synthetic seismic data.

## Wavefield simulation

We have employed the acoustic staggered-grid FD modelling for wavefield simulation and computation of full-wave synthetic seismic data for the complex graben model (Figure 10). As mentioned above for the two different models (Figures 4 and 7), we have also used the different type of boundary-conditions for this model (Figure 10) to understand the nature of wave propagation at different time-steps through the media and generation of full-wave synthetic seismic data. We have shown the wavefield simulation for the shot located at 1.5 km distance, which is the centre of this complex graben model (Figure 10) similar to the above two models. At the time-step of 0.5 s, the corresponding snapshot of the wave propagation through the model show very complex wave-front with different type of waves generated using no boundary-condition (Figure 11a), free-surface boundary-condition (Figure 11b), free-surface with absorbing-boundary-condition (Figure 11c) and free-surface with PML absorbing-boundarycondition (Figure 11d) because the wave propagation is through the vertically heterogeneous media. But we can observe that, there is comparatively very less distortions or noises of wave propagation in the snapshot for the free-surface with PML absorbing-boundary-condition (Figure 11d) as compared to no boundary-condition (Figure 11a) and other two boundary-conditions (Figure 11b, c). However, at time-step of 0.75 s, the corresponding snapshots of wave propagation show very complex nature of wavefield having different noises and spurious arrivals superimposed on the reflections from the different interfaces of the complex graben model (Figure 10) with application of all the abovementioned boundary-conditions (Figure 11e-h). It is clearly observed that, the snapshot of the wavefield using free-surface with PML absorbing-boundarycondition (Figure 11h) minimizes all the spurious arrivals, back-scattered noises, multiples and other distortion of waves as compared to the corresponding snapshots of wave propagation using other three boundary-conditions (Figure 11e-g). At increasing time steps of 1.0 s, we can see that there is more complexity of wavefield leading to spurious arrivals present in the snapshots of wave propagation having application of no boundary-condition (Figure 11i), free-surface boundarycondition (Figure 11j), free-surface with absorbingboundary-condition (Figure 11k) as compared to freesurface with PML absorbing-boundary-condition (Figure 11I).

The snapshot generated at 1.0 s show very clear downgoing waves and reflected waves with complete absorption of unwanted waves or noises using freesurface with PML absorbing-boundary-condition (Figure 11l) for the acoustic staggered-grid FD modelling. Similarly, at the final time-step of 1.25 s, the corresponding snapshot of the wave propagation has limited arrivals similar to the other two models as mentioned above at time-step of 2.0 s (Figures 5 and 8). However, we could observe the presence of some numerical phases and distortions of the wavefield in the snapshots with application of no boundary-condition (Figure 11m), free-surface boundary condition (Figure 11n), free-surface with absorbing-boundary-condition (Figure 11o) as compared to free-surface with PML absorbing-boundary-condition (Figure 11p) for the wave propagation through the media. Hence, with increasing complexity of the model, we also observe that there is no leakage of waves as well as complete absorption of unwanted arrivals and numerical phases generated due to FD modelling using the staggeredgrid scheme in the case of free-surface with PML absorbing-boundary-condition (Figure 11d, h, l, p) snapshots of the wave propagation through the complex graben model (Figure 10) indicating the efficacy of the method.

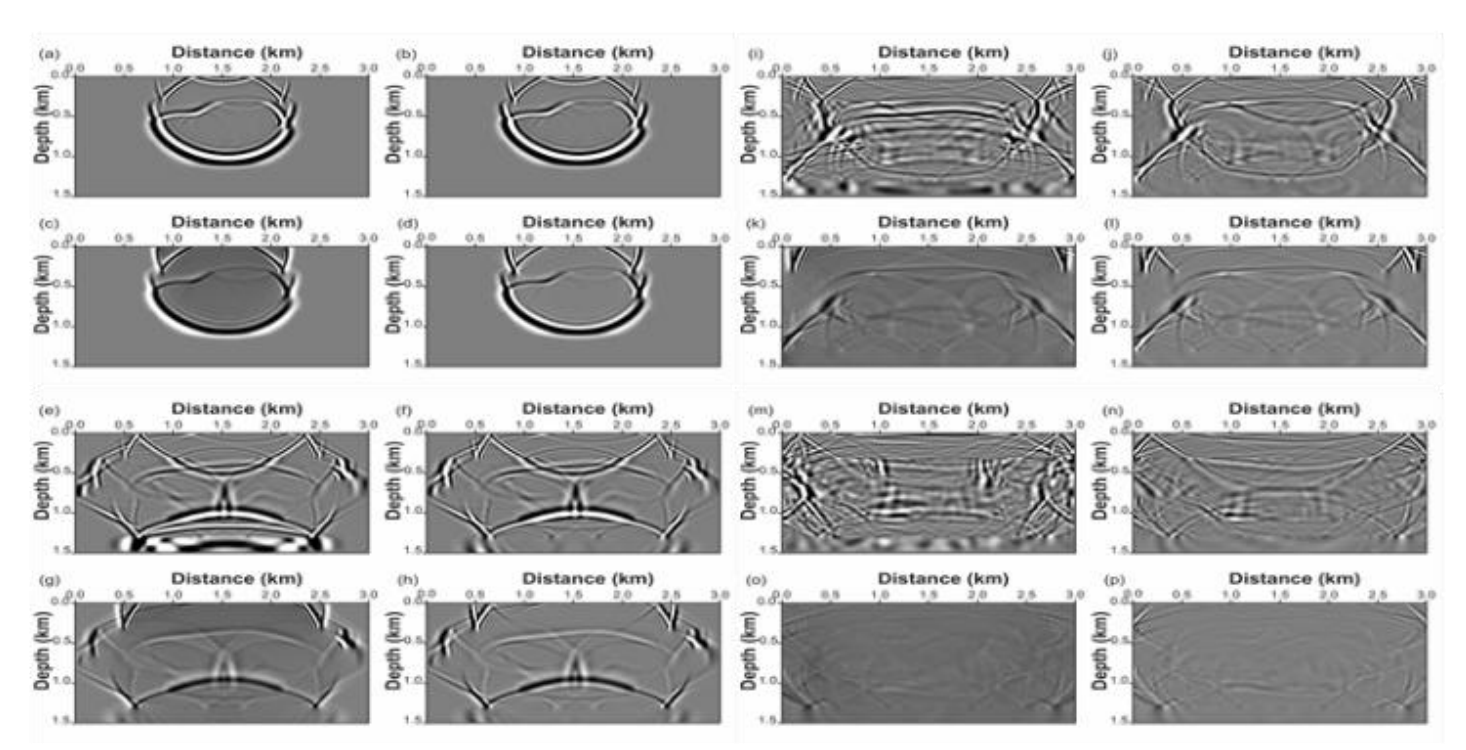


**Figure 11:** The snapshots of corresponding wavefield simulation are shown for the complex graben model (Figure 10) at different time-steps by employing the same (a) no boundary-condition, (b) free-surface boundary-condition, (c) free-surface with absorbing-boundary-condition, and (d) free-surface with perfectly-matched-layer (PML) absorbing-boundary-condition for the wave propagation at 0.5 s through the model. Similarly, the snapshots of the wave propagations at 0.75 s with the above-mentioned boundary conditions are shown in panels (e) to (h), at 1.0 s in panels (i) to (l), at 1.25 s in panels (m) to (p), respectively for this five-layer model.

The full-wave synthetic seismic data generated after complete wavefield simulation through the complex graben model (Figure 10) using no boundary-condition, free-surface boundary-condition, free-surface with absorbing-boundary-condition and free-surface with PML absorbing-boundary-condition are shown in (Figure 12a-d). There are several different types of arrivals with direct arrivals, reflections from each layer, back-scattered noises, multiples, diffractions, and several different noises are present in the computed fullwave synthetic seismic data obtained for the complex graben model having five-layers (Figure 10). The synthetic seismic data obtained without application of any boundary-condition for this model having four different reflecting interfaces (Figure 10) show various arrivals like back-scattered noises, multiples, and other numerical phases along with the direct arrivals and reflection phases (Figure 12a). However, the effect of these spurious arrivals, multiples and noises present in the data diminishes with application of free-surface

boundary-condition (Figure 12b), free-surface with absorbing-boundary-condition (Figure 12c) and free-surface with PML absorbing-boundary-condition (Figure 12d). The quality of synthetic seismic data generated by employing free-surface with PML absorbing-boundary-condition (Figure 12d) is considerably much better without any unwanted arrivals or spurious noises as compared to other three data sets (Figure 12a-c). Hence, the acoustic FD full-wave modelling using staggered-grid scheme and employing the free-surface with PML absorbing-boundary-condition can generate high quality full-wave synthetic seismic data (Figure 12d), which are generally required for optimal seismic imaging as compared to the data obtained with application of other boundary-conditions (Figure 12a-c).

## **SEISMIC IMAGING**

Seismic imaging using different migration techniques play pivotal role for delineating the subsurface geological structures. It accurately images the reflected

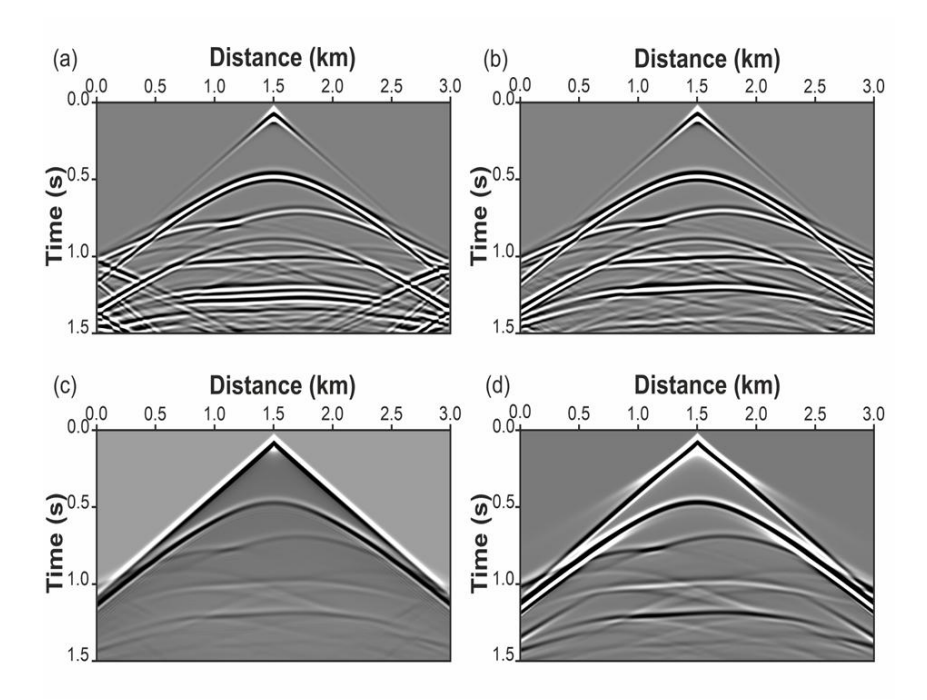


Figure 12: The acoustic full-wave synthetic seismic data computed for the shot at 1.5 km of the complex graben model (Figure 10) using the staggered-grid FD modelling scheme (Figure 1) by employing (a) no boundary-condition, (b) free-surface boundary-condition, (c) free-surface with absorbing-boundary-condition, and (d) free-surface with PML absorbing-boundary-condition, respectively. The synthetic seismic data show nature of different arrivals for the complex graben model having four different reflecting interfaces.

and diffracted energy to provide accurate structures of the geological targets of interest, which are very important for hydrocarbon exploration to find potential oil and gas bearing zones within the earth. Migration of seismic data is considered as the most compute intensive and cumbersome process in seismic data processing sequence. Seismic migration is a wave equation-based technique, which mainly attempts to attenuate all the distortions from the reflection seismic data by moving the events or reflections to their true spatial subsurface locations. Migration technique mainly tries to shorten, steepen and moves the dipping events to their true subsurface position by collapsing the diffractions or Fresnel zones observed in the seismic sections resulting accurate subsurface image having greater spatial resolution (Yilmaz, 1987). Migration is also called an inverse process in which the recorded events are back-propagated to their corresponding reflection positions.

There are several ways to migrate the seismic data. The numerical techniques employed can generally be classified into three broad categories, namely:

summation or integral methods such as Kirchhoff migration (Schneider, 1978), finite-difference methods (Claerbout, 1976, 1985), and transformation methods such as f-k migration (Stolt, 1978; Gazdag, 1978; Gazdag and Squazzero, 1984). All these migration methods make use of some approximations to the scalar wave equation. The choice of the migration method to a particular data set mainly depends upon the complexity of the velocity model. Some migrations like f-kmigration are computationally fast but can handle only the velocity variations with depth. Other migration methods like Kirchhoff, finite-difference, phase shift plus interpolation (PSPI) method can able to handle both lateral and vertical velocity variations with complex geological structures, but require large computational resources in terms of speed, memory and I/O. Migration can be performed in either time or depth (Yilmaz, 1987). In the presence of strong lateral velocity variations, time migration followed by time to depth conversion poorly image the reflected energy to its true subsurface position. Hence, the depth migration is preferred for this case. Depth migration generally compensates for ray bending, lateral velocity pull-ups and the subsurface structure. The main advantage of depth migration is that the output image is obtained in depth domain and hence, this can be directly used for geological interpretation without any conversion of seismic sections from time domain to depth domain.

For the imaging of full-wave synthetic seismic data generated, we have employed the 2-D wave-equation based finite-difference pre-stack depth migration (FDMIG) of different models (Figures 4, 7 and 10) used in our study. The FD pre-stack depth migration offers significant improvement over the Kirchhoff and f-k migrations for imaging the complex geological structures although computationally very expensive. We have used the synthetic seismic data generated using acoustic FD full-wave modelling by employing the freesurface with PML absorbing-boundary-conditions corresponding to the three different models (Figures 4, 7 and 10) for the FDMIG because of the data quality. The theory of application for the FDMIG can be briefly described based on the pioneering works of Claerbout (1985), Yilmaz (1987), and Li (1991). Assuming that seismic wave propagation in the earth follows the scalar acoustic wave equation:

$$\frac{\partial^2 P}{\partial x^2} + \frac{\partial^2 P}{\partial y^2} + \frac{\partial^2 P}{\partial z^2} = \frac{1}{V^2(x, y, z)} \frac{\partial^2 P}{\partial t^2},\tag{16}$$

where P(x,y,z,t) is the pressure and V(x,y,z) is the acoustic velocity of the media. The equation (16) is transformed to the Helmholz equation by assuming that the wave propagation occurs approximately along the z-axis, then we can obtain the corresponding paraxial wave equation (Claerbout, 1985; Yilmaz, 1987; Li, 1991) as:

$$\frac{\partial P}{\partial z} = \pm \frac{i\omega}{V(x,y,z)} \sqrt{1 + \frac{V^2(x,y,z)}{\omega^2} \left(\frac{\partial^2}{\partial x^2} + \frac{\partial^2}{\partial y^2}\right)} P$$
 (17)

where  $\omega$  is the frequency of the propagating wave. The positive and negative signs of equation (17) correspond to upcoming and downgoing wavefields. In fact, the two waves propagate through the medium independently, but the one-way method focuses on the primary arrival, not on the result of any internal reflections within the model, so the upcoming waves are ignored, only the positive sign part of equation (17) is kept for FDMIG. Hence, we only use the downgoing waves in the wavefield continuation depth migration. The evaluation

of the square-root operator is numerically difficult, hence it is approximated by a series that has its origin in a continued-fraction expansion (Claerbout, 1985; Yilmaz, 1987). The continued-fraction expansion can be represented by ratios of polynomials (Ma, 1981) and the polynomial coefficients can be optimized propagation angle (Lee and Suh, 1985). computational efficiency and numerical speed, the continued-fraction expansion is split to separate the operators in the x and y directions. This produces an equation with the three terms, which can be solved individually using the method of fractional steps. The first-term is the thin-lens term and involves a solution of a complex exponential. The second and third terms are the diffraction terms for the x and y directions, which require efficient tridiagonal solutions across the solution domain. The approximation of the square-root operator, and the splitting step operator introduce errors into the migration. Two different filters have been provided in the paraxial equation (17) to correct for these approximations. The Graves and Clayton filter (Graves and Clayton, 1990) corrects for errors introduced by the operator splitting, and the Li filter (Li, 1991) attempts to correct for both approximations. Finally, we apply the absorbing-boundary-conditions similar to described in Clayton and Engquist (1980) and Xu (1996). Thus, the overall procedure of solution is to read the data in a velocity plane, then compute the thin-lens and diffraction terms, correct for errors using one of the above filters, then apply an imaging condition to produce an image, and finally write this image to disk.

This is repeated for each depth-step as we march down into the subsurface earth. The detail steps of the processing flow to obtain the final FDMIG image is shown in Figure 13. The results obtained by employing FDMIG to the full-wave synthetic seismic data obtained with free-surface and PML absorbing-boundary-conditions for the flat-horizontal model (Figure 4), syncline and anticline model (Figure 7) and the complex graben model (Figure 10) are shown in Figure 14. We have used total thirty-one full-wave synthetic shot-gathers generated (Table-1) using staggered-grid acoustic FD modelling by employing free-surface PML absorbing-boundary-condition (Figure 6) for imaging the flat-horizontal model (Figure 4) with the help of acoustic FDMIG (Figure 13). The image obtained show

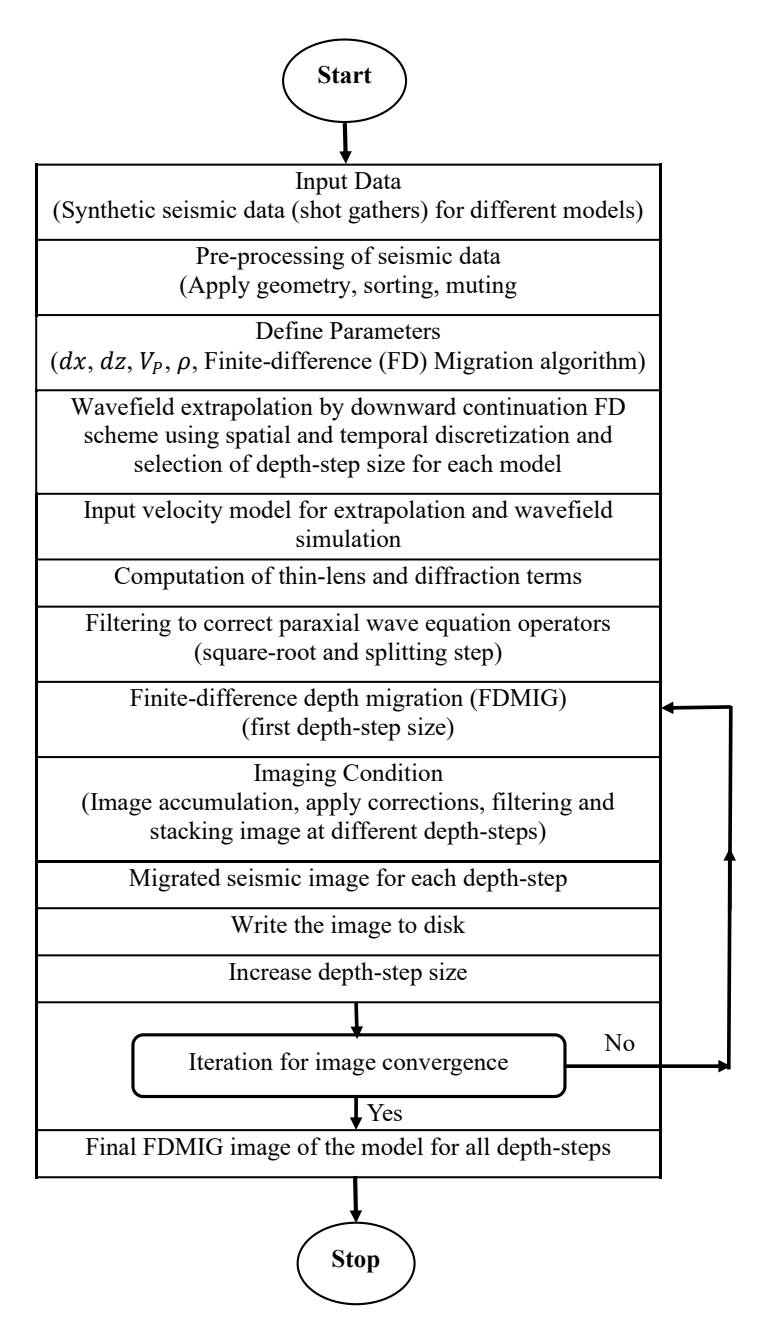


**Figure 13.** The processing workflow for 2-D wave-equation based finite-difference pre-stack depth migration (FDMIG) used for imaging the acoustic full-wave synthetic seismic data computed by staggered-grid FD modelling and employing free-surface with PML absorbing-boundary-condition for three different models (Figures 4, 7, and 10).

very clear reflecting horizon at 1.0 km depth (Figure 14a) without any distortions or noises, which generally occur at the edges of the model boundaries. The depth-step size used for the migration of synthetic seismic data for the flat-horizontal model (Figure 4) is 2 m for optimal seismic imaging. The depth-step size ( $\Delta z$ ) is generally computed using the formula  $\Delta z = V_{min}/4f_{max}$  (Yilmaz,

1987). For the flat-horizontal model, the minimum value of  $V_P$  is 2.0 km/s and maximum frequency ( $f_{max}$ ) used is 250 Hz (i.e. Nyquist frequency corresponds to half the sampling rate) for sampling rate of 2 ms corresponding to the data generated. Hence, the depth-step size computed is 2 m. For the FDMIG, the depth-step size is a very critical parameter that affects the quality of the

migrated image. A smaller depth-step size used in FDMIG can provide an accurate image with increasing cost of computational time, while a larger depth-step size can save computational resources and time but simultaneously may introduce several artifacts or undermigration. The optimal depth-step size needs to trade-off between the accuracy and computational efficiency. It should be small enough to avoid significant artifacts and aliasing, but large enough to minimize the computational cost. Hence, the optimal depth-step size is generally chosen based on the specific characteristics of the data, the velocity model, and the desired image quality.

Similarly, for the syncline and anticline model (Figure 7), we have applied the acoustic FDMIG processing flow (Figure 13) for the same thirty-one full-wave synthetic shot gathers generated (Table-1) using staggered-grid acoustic FD modelling by employing free-surface PML absorbing-boundary-condition (Figure 9). The depthstep size of 2 m is obtained using minimum velocity  $V_P$ of 2.0 km/s and maximum frequency  $f_{max}$  of 250 Hz for sampling rate of 2 ms. The corresponding FDMIG image for the syncline and anticline model (Figure 7) is shown in Figure 14b, which clearly delineate the syncline and anticline structure with correct positioning of the reflection events without any artifacts or noises due to the migration errors. Hence, the depth-step size chosen is optimal and minimized the artifacts generated during the migration with computational efficiency (Figure 14b).

The complex graben model (Figure 10) with application of acoustic FDMIG (Figure 13) for the forty-seven fullwave synthetic shot gathers generated (Table-1) using staggered-grid acoustic FD modelling by employing free-surface PML absorbing-boundary-condition (Figure 12) show very clear image of all the structures (Figure 14c). The corresponding depth-step size of 3 m is obtained using minimum  $V_P$  of 1.5 km/s and maximum frequency  $f_{max}$  of 125 Hz for sampling rate of 4 ms. The FDMIG image obtained for the complex graben model (Figure 10) is shown in Figure 14c, which clearly depicts all the complex subsurface structures with proper positioning of the reflection events. There are very less artifacts, distortions or noises present in the seismic image, which are obvious due to the complexity of the model having four different reflecting interfaces with substantial velocity variations through the different layers. It is also important to note that the steeply dipping reflectors of the graben along with the flathorizontal reflector beneath this are well positioned in depth without much distortions and velocity pull-up, which generally occur if other migration techniques are used. The alternate syncline and anticline feature present above the graben structure are also very well resolved and positioned accurately in depth without any artifacts or distortions. The flat-horizontal reflector above the alternate syncline and anticline structure is also very well imaged with proper positioning in depth. Hence, all the structural features imaged are well focused and accurate with correct positioning in the depth (Figure 14c). This indicates that the depth-step size chosen is optimal and minimized the artifacts generated during the migration with computational efficiency for this complex graben model.

## **CONCLUSIONS**

Simulation of seismic wavefield using acoustic staggered-grid finite-difference scheme plays a very important role for generation of full-wave synthetic seismic data. We have used this scheme for different models like flat-horizontal layer model, syncline and anticline model, and complex graben model for wavefield simulation and generation of full-wave synthetic seismic data. While performing wavefield simulation through these different models, we have also shown the wave propagation at different time-steps using no boundary-conditions, free-surface boundaryconditions, free-surface with absorbing-boundaryconditions, and free-surface with PML absorbingboundary-conditions to illustrate the nature of wave propagation from the snapshots taken for the three benchmark models with increasing complexity. We have also computed the acoustic full-wave synthetic seismic data for these three models using the different boundary-conditions, which implied that application of free-surface with PML absorbing-boundary-condition has superior data quality as compared to the other three types of boundary-condition. The synthetic seismic data using free-surface with PML absorbing-boundarycondition are devoid of different types of noise and considerably better data quality without any unwanted arrivals or spurious noises as compared to other three data sets. Hence, the acoustic FD full-wave modelling

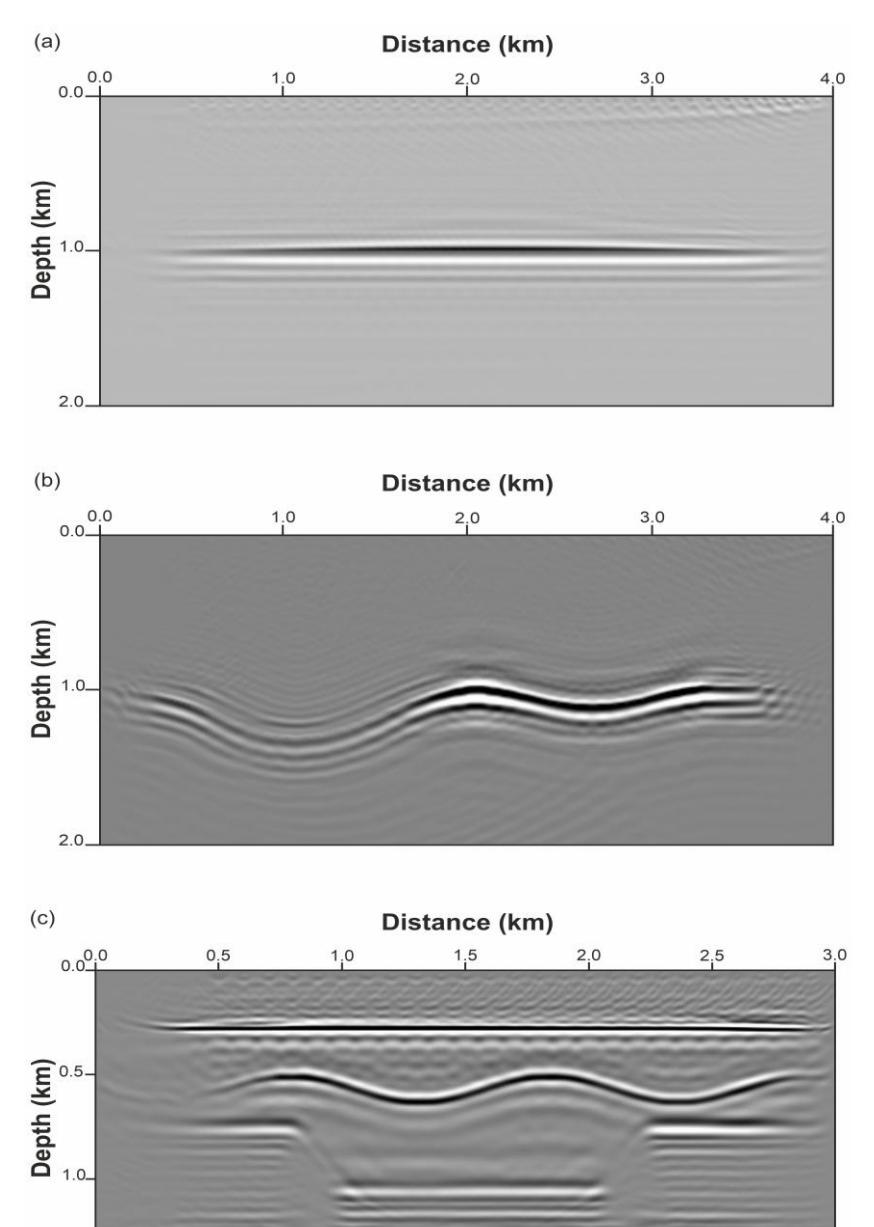


**Figure 14.** The corresponding FDMIG image obtained for (a) flat-horizontal model, (b) syncline and anticline model, and (c) complex graben model. The image shows accurate positioning of the different reflecting horizons without much distortions for all the three models and no velocity pull-ups below the steeply dipping reflectors for the complex graben model indicating the robustness and efficacy of the FDMIG for imaging the complex geological structures.

using staggered-grid scheme and employing the freesurface with PML absorbing-boundary-condition can generate high quality full-wave synthetic seismic data, which are required for optimal seismic imaging as compared to the other synthetic data obtained for these models having spurious arrivals and different type of noises predominant along with the required seismic reflection arrivals. For optimal seismic imaging using the full-wave synthetic seismic data computed using the free-surface with PML absorbing-boundary-condition for different models of this study, we have employed the robust and highly compute intensive and accurate 2-D wave-equation based FDMIG for seismic imaging. The corresponding FDMIG images show accurate positioning of the reflectors corresponding to different geological structures like flat-horizontal model, syncline and anticline model, and the complex graben model of this study having minimum artifacts and distortions without any velocity pull-up below the steeply dipping reflectors. This indicates that the migration algorithm

used in this study is numerically stable and efficient to suppress the noises generally occur due to migration errors leading to very good focusing and proper positioning of all the reflection events in their true subsurface position. *G* 

#### **ACKNOWLEDGEMENTS**

We thank Dr. Prakash Kumar, Director, CSIR-NGRI to accord permission for publication of this paper. ARB

#### **REFERENCES**

Bartolo, L. D., D. Celeberson, and W. J., Mansur, 2012, A new family of finite-difference schemes to solve the heterogeneous acoustic wave equation, Geophysics, **77**(5), T187-T199. <a href="https://dois.org/10.1190/GEO2011-0345.1">https://dois.org/10.1190/GEO2011-0345.1</a>

Behera, L., 2022, Elastic anisotropic finite-difference full-wave modelling and imaging of 2D tilted transversely isotropic (TTI) media, J. Appl. Geophys., **207**(104837), 1-24. <a href="https://doi.org/10.1016/j.jappgeo.2022.104837">https://doi.org/10.1016/j.jappgeo.2022.104837</a>

Behera, L., and I. Tsvankin, 2009, Migration velocity analysis for tilted transversely isotropic media, Geophys. Prosp., **57**, 13-26. <a href="https://doi.org/10.1111/j.1365-2478.2008.00732.x">https://doi.org/10.1111/j.1365-2478.2008.00732.x</a>

Claerbout, J. F., 1976, Fundamentals of Geophysical data processing, McGraw Hill Inc.

Claerbout, J. F., 1985, Imaging the Earth's Interior, Blackwell Scientific Publications, Boston.

Clayton, R., and B. Engquist, 1980, Absorbing boundary conditions for wave-equation migration, Geophysics, **45**(5), 895-904. https://doi.org/10.1190/1.1441094

Collino, F., C. Tsogka, 2001, Application of the PML absorbing layer model to the linear elastodynamic problem in anisotropic heterogeneous media, Geophysics, **66**(1), 294-307. <a href="https://doi.org/10.1190/1.1444908">https://doi.org/10.1190/1.1444908</a>

Courant, R., K. Friedrichs, and H. Lewy, 1967, On the partial difference equations of mathematical physics, IBM Journal, English translation of the 1928 German original, 215-234. <a href="https://www.stanford.edu/class/cme324/classics/courant-friedrichs-lewy.pdf">https://www.stanford.edu/class/cme324/classics/courant-friedrichs-lewy.pdf</a>

Fornberg, B., 1988, Generation of finite difference formulas on arbitrarily spaced grids, Mathematics of Computation, **51**(184), 699-706.

Gazdag, J., 1978, Wave equation migration with the phase-shift method, Geophysics, **43**(7), 1342-1351. https://doi.org/10.1190/1.1440899

thanks AcSIR, CSIR-NGRI for pursuing his Ph. D. We sincerely thank Dr. Ranjit K. Shaw for his constructive and thought-provoking comments and Satinder Chopra, Chief-Editor, GEOHORIZONS for suggestions and modifications to improve the quality of the paper.

This work is the scientific research contribution of CSIR-NGRI under GAP-826-28 (LB) with Ref. No.: NGRI/Lib/2025/Pub-76.

Gazdag, J., and P. Sguazzero, 1984, Migration of seismic data by phase shift plus interpolation, Geophysics, **49**(2), 124-131. https://doi.org/10.1190/1.1441643

Graves, R. W., 1996, Simulating seismic wave propagation in 3D elastic media using staggered-grid finite differences, Bull. Seismolo. Soc. Am., **86**, 1091-1106.

Graves, R. W., and R. Clayton, 1990, Modeling acoustic waves with paraxial extrapolators, Geophysics, **55**(3), 1650-1660. https://doi.org/10.1190/1.1442838

Lee, M., and S. Suh, 1985, Optimization of one-way equation, Geophysics, **50**(10), 1634-1637. https://doi.org/10.1190/1.1441853

Levander, A. R., 1988, Fourth-order finite-difference P-SV seismograms, Geophysics, **53**(11), 1425-1436. <a href="https://doi.org/10.1190/1.1442422">https://doi.org/10.1190/1.1442422</a>

Li, Z., 1991, Compensating finite-difference errors in 3-D migration and modelling, Geophysics, **56**(10), 1650-1660. https://doi.org/10.1190/1.1442975

Ma, Z., 1981, Finite-difference migration with higher-order approximation, Joint meeting of Chinese Geophys. Soc., and Soc. Explor. Geophys., Society of Exploration Geophysicists.

Schneider, W. A., 1978, Integral formulation for migration in two and three dimensions, Geophysics, **43**(1), 49-76. https://doi.org/10.1190/1.1440828

Sei, A., 1995, A family of numerical schemes for the computation of elastic waves, SIAM J. Sci. Comp., **16**(4), 898-916.

Stolt, R. H., 1978, Migration by Fourier transform, Geophysics, **43**, 23-48.

Thorbecke, J., 2017, 2D finite-difference wavefield modelling, Unpublished Report, 1-68.

Virieux, J., 1984, SH-wave propagation in heterogeneous media: Velocity-stress finite-difference method, Geophysics, **49**(11), 1933-1957. <a href="https://doi.org/10.1190/1.1441605">https://doi.org/10.1190/1.1441605</a>

Virieux, J., 1986, P-SV wave propagation in heterogeneous media: Velocity-stress finite difference method, Geophysics, **51**(4), 889-901. <a href="https://doi.org/10.1190/1.1442147">https://doi.org/10.1190/1.1442147</a>

Xu, L., 1996, Working notes on absorbing boundary conditions for prestack depth migration, Personal Communication.

Yilmaz, O., 1987, Seismic Data Processing, Investigations in Geophysics No. 2, Society of Exploration Geophysicists, Tulsa, OK, USA.

#### **BIOGRAPHIES**



**Raju Babu Allu** is a highly motivated researcher in the Controlled Source Seismic (CCS) Group at CSIR-NGRI, Hyderabad, with over 7 years of expertise in seismic modelling, imaging, and inversion. He received his B. Sc. from Dr. V. S. Krishna Govt. Degree College, Andhra University, and M. Sc. Tech. in Geophysics from Andhra University. He is currently pursuing his Ph. D. in AcSIR at CSIR-NGRI. He has expertise in land and marine (2D, 3D) seismic data acquisition, processing, and interpretation, as well as modelling and inversion of seismic data. He is proficient with different programming languages, particularly in C, C++, and Fortran, as well as a strong background in numerical geophysics. He is presently involved in seismic imaging with application of full-wave modelling/inversion and reverse time migration (RTM) techniques to both synthetic and real data sets.



**Dr. Laxmidhar Behera** serves as the Chief Scientist of the CSS Group and is a Professor at AcSIR, CSIR-NGRI, Hyderabad, having 25 years of R&D experience. He has authored 41 SCI-indexed publications and a book. His significant contributions span seismic data acquisition (CDP and wide-angle using 1C and 3C) for hydrocarbon exploration and crustal studies, as well as advanced seismic data processing and interpretation. His expertise is mainly focused on seismic imaging, modeling and inversion, tomography, anisotropic depth imaging for VTI and TTI media, sub-basalt imaging in DVP, basin modeling, tectonics and geodynamics with emphasis on the Moho configuration of India. Laxmidhar received his B.Sc. in Physics from Utkal University, M.Sc. Tech. in Geophysics from IIT-ISM, Dhanbad, Ph.D. in Exploration Geophysics from Osmania University, Hyderabad, and postdoctoral fellowship from CWP, CSM, USA. He has been honoured with numerous awards such as the Dr. Hari Narain Gold Medal by MGMI Kolkata, the ONGC-AEG Best Ph.D. Thesis Award, a USGS Fellowship in the USA, a

BOYSCAST Fellowship by DST, Krishnan Gold Medal from IGU, along with the Young Scientist Award from SERC-DST and fellow of IGU. He has also served as a visiting scientist at USGS, CSM, and Nanometrics.